FACTA UNIVERSITATIS
Series: **Mechanical Engineering** Vol. 23, No 4, 2025, pp. 921 - 943
https://doi.org/10.22190/FUME250830033C

Review article

CU-CU MECHANICAL BONDING FOR 3D INTEGRATION OF THE NEXT GENERATION ELECTRONIC CHIPS: INTERFACIAL MECHANISMS, SURFACE ENGINEERING, AND EMERGING LOW-TEMPERATURE STRATEGIES

Sooyong Choi[1], Chih-Ming Chen[2], Byungil Hwang[3]

[1]Department of Intelligent Semiconductor Engineering,
Chung-Ang University, Republic of Korea
[2]Department of Chemical Engineering, National Chung Hsing University, Taiwan
[3]School of Integrative Engineering, Chung-Ang University, Republic of Korea

ORCID iDs: Sooyong Choi https://orcid.org/0009-0004-1523-4122
Chih-Ming Chen https://orcid.org/0000-0003-4481-1094
Byungil Hwang https://orcid.org/0000-0001-9270-9014

Abstract. *Three-dimensional integrated circuit (3D IC) technology is essential for ultra-high-density integration, and Cu-Cu direct mechanical bonding has emerged as a promising alternative due to the limitations of traditional soldering methods. This technology offers excellent power efficiency, high-density packaging, faster processing speeds, and improved heat dissipation. However, existing research has limitations in systematically analyzing the relationship between key parameters affecting Cu-Cu bonding quality such as bonding layer thickness, temperature, grain size, and surface roughness. A comprehensive review, particularly under the low-temperature conditions necessary for 3D IC processes, has been lacking. Therefore, this review introduces the fundamental theory of Cu-Cu bonding and systematically discusses the effects of the parameters on bonding quality. By integrating these factors with a specific focus on low-temperature Cu-Cu interfaces, this review aims to provide a practical and up-to-date guide on Cu-Cu bonding technologies.*

Key words: *Cu, Bonding, 3D Packaging, Low-temperature bonding*

1. INTRODUCTION

Technological advancements in computing and data storage systems have driven the demand for ultra-high-density integrated circuits. Over the past few decades, reducing the transistor size has been the primary focus of research and development in the high-density integrated circuit (IC) field. The current state-of-the-art scaling technologies have achieved

Received: August 30, 2025 / Accepted November 10, 2025
Corresponding author: Byungil Hwang
School of Integrative Engineering, Chung-Ang University, Seoul 06974, Republic of Korea
E-mail: bihwang@cau.ac.kr

gate widths in the range of just a few nanometers [1-3]. However, further size reduction presents significant challenges owing to the quantum mechanical limitations of these materials [4]. Consequently, the interest in three-dimensional (3D) IC technology has increased in recent years. 3D ICs maximize the chip density by stacking multiple chips vertically on a limited substrate area, with high bandwidth memory (HBM) being a prime example [5-8]. In HBMs, 16-high stacks have been formed to achieve dynamic random access memories (DRAM) with 32 GB capacity.

Traditionally, chip-to-chip connections have been created using external metal solder balls [9-18]. However, in 3D ICs, where the gaps between the interconnections are in submicron scales, conventional soldering techniques become increasingly challenging. This has led to a growing interest in direct bonding technologies, where metal interconnects are bonded without the need for external solder balls [14-18]. Among the various interconnect materials such as Ag, Au, and Cu, Cu-Cu direct bonding stands out because of Cu's exceptional mechanical properties, superior electromigration resistance, high electrical conductivity, and excellent thermal conductivity. Additionally, Cu's cost-effectiveness, compared with that of Au and Ag, makes it the preferred choice in industrial applications. Consequently, Cu-Cu bonding has become the most widely adopted technology for packaging in 3D ICs [19-24].

In Cu-Cu direct bonding, two flat Cu surfaces are joined at high temperatures by applying external pressure. A bond is formed through the diffusion of atoms and grain growth between the surfaces. Surface diffusion plays a critical role in facilitating Cu-Cu bonding as Cu atoms migrate across the interface, forming a bonded structure. As the process continues, recovery and grain growth at both the interface and interior of Cu further enhance the bond [25-27]. The quality of this bond is primarily determined by the bonding conditions such as time, temperature, pressure, and initial surface and microstructural characteristics of Cu [28]. Therefore, a thorough understanding of how these factors influence the bonding properties is essential to achieve high-quality Cu-Cu bonding.

Despite the increasing focus on developing reliable Cu-Cu bonding technologies, comprehensive reviews that address the critical factors affecting the bonding reliability are lacking. This review explores the fundamental mechanisms and theoretical background of Cu-Cu bonding under various conditions. It also highlights the state-of-the-art surface control technologies used to achieve high-quality Cu-Cu bonds at low temperatures, offering a future perspective on the role of Cu-Cu bonding in the next-generation electronic packaging.

2. Factors Affecting Cu-Cu Mechanical Bonding

The grain size and surface roughness of Cu are crucial factors for achieving high-quality bonding interfaces [28-38]. A reduction in the grain size decreases the likelihood of microcracks, thereby enhancing the shear strength. Grain boundaries act as barriers to crack propagation; therefore, smaller grain sizes at the Cu-Cu bonding interface result in stronger bonds [39]. This relationship is described by the Hall–Petch equation,

$$\sigma_y = \sigma_{y,0} + kd^{-0.5} \tag{1}$$

where σ_y is the yield strength related to the grain size, $\sigma_{y,0}$ is the starting yield stress for dislocation movement, k is a constant of strengthening coefficient, and d is the average grain size [40].

Kao et al. [41] confirmed the Hall–Petch relationship in electrically plated Cu thin films. This directly supports the validity of the premise that "smaller grain size → higher yield strength/hardness of the material itself" in Cu. Grain size and mechanical response co-vary, and smaller grains tend to accompany higher yield stress. Table 1 shows the electron backscatter diffraction (EBSD) mapping and its summary for various Cu electroplated samples with different bis-(3-sulfopropyl) disulfide (SPS) conditions. PC designates specimens electroplated with polyethylene glycol (PEG) and chloride ions, whereas PCS refers to those containing SPS as an accelerator in addition to the PC composition. PC, PCS0.2, PCS0.5, PCS1.0, and PCS2.0 represent samples with increasing SPS concentration, from 0 ppm (PC) to 2.0 ppm (PCS2.0). The results indicate that PCS0.2 exhibits the smallest average grain size (0.29 μm), while higher SPS specimens show larger grains (Table 1, Fig. 1). Consistently, tensile data report the highest average yield stress for PCS0.2, with lower values for the coarser-grained specimens (Table 2), in agreement with the Hall–Petch relation. These results suggest that grain refinement likely contributes to boundary strengthening and the observed increase in yield stress within this dataset.

Table 1 Average grain sizes of various Cu electroplated samples determined by the EBSD grain mappings in Fig. 1

Specimens	PC	PCS0.2	PCS0.5	PCS1.0	PCS2.0
Grain size (μm)	0.55	0.29	1.97	3.79	3.77

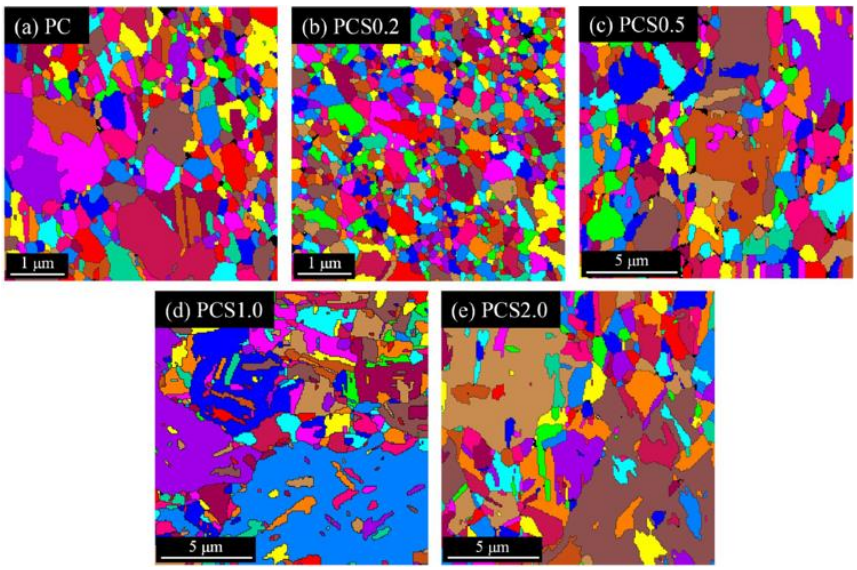

Fig. 1 EBSD grain mappings of the Cu electroplated layers labelled as (a) PC, (b) PCS0.2, (c) PCS0.5, (d) PCS1.0, and (e) PCS2.0. The mappings are created by orientation imaging microscopy (OIM) Analysis v8 [41]

Table 2 Yield stresses and elongations of various Cu electroplated samples

Specimens	PC	PCS0.2	PCS0.5	PCS1.0	PCS2.0
Yield Stress (MPa)	351 ± 8	416 ± 8	290 ±12	261 ± 5	248± 2
Elongation (%)	2.9 ± 0.2	4.3 ± 0.3	7.2 ± 0.9	9.0 ± 0.7	9.4 ± 0.4

Somekawa et al. [42] studied the effect of grain size on the shear strength, bonding time, and bonding pressure by comparing two types of samples: a fine-grained sample with an 11 μm grain size and a coarse-grained sample with a 28 μm grain size. They found that, to achieve a comparable shear strength, the coarse-grained sample required thermal pressing for 3 h at 5 MPa, whereas the fine-grained sample required pressing for only 2 h at 3 MPa [42]. This indicated that finer grain sizes contributed to higher bond strengths under the same temperature, pressure, and time conditions.

In general, in Cu, there is a tendency for "fine grains → bonding promotion." However, locally, there are cases where adhesion weakens at defect concentration points such as grain boundaries and triple points, so we must be cautious about the equation "many grain boundaries are equal to strong adhesion." As shown in Fig. 2, this is a regional property that varies significantly depending on location and microstructure, so generalization should be avoided [43]. For example, in Fig. 2 (d), it can be observed that the adhesion strength at the junction area is significantly reduced.

The surface roughness also significantly affects bond quality. To achieve high-quality bonding, it is critical to maximize the actual contact area between the two metal surfaces. Gui et al. [44] demonstrated a strong correlation between the bonding energy and actual contact area. Excessive roughness could promote void formation, which reduced the mechanical strength [45]. In the work by Rebhan et al. [39], the bonding strength linearly increased as the roughness decreased from 8.0 to 1.5 nm. Shigetou et al. [46] demonstrated that chemical mechanical polishing (CMP) polished Cu films with a mean surface roughness of approximately 0.3 nm could be directly bonded at room temperature via the surface activated bonding (SAB) method. Under a background vacuum below $\sim 3\times10^{-3}$ Pa, these atomically smooth surfaces achieved full-area atomic-level bonding between Cu grains with shear strengths exceeding 50 MPa. Thus, optimizing the surface roughness is essential for maximizing the bonding strength of Cu-Cu bonding.

As mentioned earlier, the bonding temperature, pressure, and time determine the degree of diffusion, which directly affects the interface quality of Cu-Cu joints. Atoms in solid metals vibrate constantly, and their kinetic energy is proportional to the absolute temperature [26]. This energy distribution allows atoms to diffuse across lattice points when they exceed a specific energy threshold. The diffusion process can be described by Fick's first law [47].

From an atomic perspective, the heat energy accumulates as the temperature increases, causing the atoms to vibrate more intensely. This increased vibration allows the atoms to move more easily from their original positions, thereby facilitating greater diffusion. In other words, atomic vibration is proportional to the temperature; thus, higher temperatures result in faster diffusion and stronger bonds. Therefore, increasing the bonding temperature enhances the diffusion of atoms and improves the bond strength between the two Cu surfaces.

Jang et al. [48] studied the effects of bonding and annealing temperatures on Cu-Cu bonding. They measured the interfacial adhesion energy after bonding at 300, 350, and 400 °C for 1 h, without annealing. The interfacial adhesion energy increased with the bonding

temperature, showing a positive correlation. At 400 °C, a small error margin was obtained, indicating uniform bonding across the wafers.

The annealing temperature also plays a crucial role in Cu-Cu bonding [28, 49, 50]. Without annealing, voids are often present at the bonding interface. However, annealing at higher temperatures produces clean Cu bonding layers. Samples were annealed at 200, 250, and 300 °C for 1 h in an N_2 environment and the results of interfacial adhesion-energy measurements were compared. Annealing at 200 °C had little effect; however, annealing at 250 and 300 °C increased the adhesion energy by 3.1 and 4.3 times, respectively [48]. These results show that, beyond a certain threshold, annealing significantly improves the adhesion energy at the Cu bonding interface when conditions such as oxygen, pressure, and time are controlled [48].

Lin et al. [51] investigated low-temperature Cu-Cu direct mechanical bonding using CMP highly (111)-oriented nanotwinned Cu (nt-Cu) films in the temperature range of 150–200 °C, and quantitatively evaluated the interfacial void distribution by cross-sectional focused ion beam (FIB) imaging. As shown in Fig. 2 (a), for the bonding condition of 150 °C for 60 min, the columnar microstructure of the nt-Cu films remains essentially intact, while a small number of tiny voids are still present along the bonding interface. In contrast, Fig. 2 (c,d) demonstrates that, when the same CMP nt-Cu films are bonded at 200 °C for 30 min, no discernible voids are observed at the Cu-Cu interface and a continuous, flat bonding interface is obtained. These observations indicate that, under identical surface roughness and bonding pressure, increasing the bonding temperature from 150 to 200 °C together with a sufficient bonding time effectively eliminates interfacial voids and improves the metallic continuity across the interface, which is expected to result in a significant enhancement of the practical bonding quality and interfacial adhesion/strength. Furthermore, Fig. 2 (b), corresponding to the condition of 200 °C for only 5 min, still exhibits a noticeable population of nanoscale voids at the bonding interface, corroborating that not only temperature but also the overall thermal budget (i.e., the temperature–time product) is a critical factor governing void healing by Cu diffusion and creep during Cu-Cu bonding.

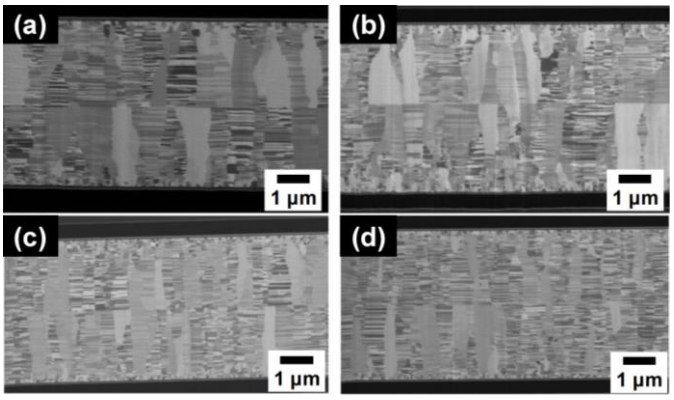

Fig. 2 Cross-sectional FIB image of the typical CMP nt-Cu films bonded at (a) 150 ◦C for 60 min and (b) 200 ◦C for 5 min. (c,d) the typical CMP nt-Cu films bonded at 200 ◦C for 30 min [51]

Li et al. [52] found a proportional relationship between the bonding pressure and shear strength in Cu nanosolder paste bonding, where higher pressures generated stronger bonds at the same temperature. These studies demonstrated that both the bonding and annealing temperatures, as well as the bonding pressure, significantly influenced the quality and strength of the Cu-Cu bonding.

Voids at the metal-metal bond interface play a critical role in determining the bonding strength [53, 54]. Even with the same overall void fraction, variations in the void shape and distribution can lead to different bonding outcomes [55]. Therefore, understanding how the status of voids affects the strength of Cu-Cu bonding is essential. Voids reduce the contact area between the metal interfaces, which in turn decreases the bonding strength and increases the resistance [56].

Oh et al. [57] investigated the effects of temperature and pressure on the formation of local voids during Cu-Cu bonding. Their results showed that increasing the pressure relative to the temperature significantly reduced the void size. Specifically, the length and height of the voids decreased markedly when the pressure was increased to 30 MPa from 20 MPa. In contrast, increasing the temperature from 200 to 300 °C led to only minor reductions in the void size. Void shapes are classified into three main categories: oblate, spherical, and prolate [58]. As the pressure decreased, the voids changed from oblate to spherical. These findings were consistent with that of other researchers who used both experimental and simulation methods [58, 59]. Additionally, a simulation study revealed that under identical conditions, oblate voids grew faster than spherical voids, and spherical voids grew faster than prolate voids, during the bonding process. The study also found that the fracture initiation toughness was the highest when the void was prolate and lowest when it was oblate. In other words, the bonding was the most robust when the void was prolate and the weakest when it was oblate [58].

Unfortunately, the voids formed at the bonding interface are usually oblate or spherical; therefore, more attention should be paid to the void formation and evolution during the Cu-Cu direct bonding process [58, 61-63]. Void ripening was observed at the bonding interface subjected to thermal annealing at 200 °C for 30 to 120 min [63]. The absence of intergranular coarsening or interface breakup indicates that the microstructural change is dominated by void evolution rather than bulk recrystallization or grain growth. Concomitantly, the void morphology evolves toward more circular shapes at longer times, with an apparent increase in the thickness dimension inferred from cross-sectional contrast. Such circularization and coarsening of a subset of voids, together with the reduction in the count of smaller voids, is the characteristic fingerprint of curvature driven Ostwald ripening at the bonding interface. The combined observations—decreasing void count with time, progressive circularization and coarsening of the surviving voids, and the lack of concurrent grain growth—substantiate the claim that void ripening occurs at the bonding interface during annealing at 200 °C for 30–120 min.

A kinetic model was proposed to describe the relationship between the void radius and annealing time. A different void evolution phenomenon was observed under nanocrystalline Cu bonding conditions [64]. The high thermal instability of nanocrystalline Cu facilitated the grain growth and amalgamation at the bonding interface at low temperatures. However, the grain growth exerted a force on the voids, which split the initial large void into numerous nanovoids. These factors such as temperature and pressure can affect the formation of these voids, so care must be taken when joining Cu-Cu interface.

In summary, the reliability of direct Cu-Cu bonding is dictated by the coupled influence of four interdependent factors—grain size, surface roughness, thermo-mechanical processing parameters, and interfacial void behavior. Refinement of the copper grain structure activates Hall–Petch strengthening, thereby elevating interfacial shear strength and suppressing micro-crack propagation under identical thermal and pressure conditions. Sub-nanometer surface roughness maximizes real contact area and therefore bonding energy, yet once a critical roughness threshold is exceeded, asperity-induced void formation offsets these benefits and degrades mechanical integrity. Because the lattice diffusion coefficient follows an Arrhenius relationship, concurrent application of moderately elevated temperatures (≈ 300–400 °C) and compressive stresses on the order of several tens of megapascals accelerates interfacial diffusion and markedly increases adhesion energy. Nevertheless, voids persist as dominant reliability hazards; while elevated temperature enhances atomic mobility, empirical evidence indicates that increased external pressure more effectively collapses or heals voids, thereby restoring contact area and lowering electrical resistance. Collectively, these observations establish a practical design framework—fine-grained microstructure, ultra smooth surfaces, judicious thermo-mechanical loading, and proactive void mitigation—through which high-integrity Cu-Cu interconnections can be consistently achieved.

3. Low-Temperature Cu-Cu Mechanical Bonding Technologies

3.1. Surface Activated Mechanical Bonding

SAB combines two materials by leveraging the interatomic adhesion of atomically clean surfaces in an ultra-high vacuum (UHV) environment at 21-25 °C [60-64]. Unlike the traditional bonding methods, SAB achieves strong bonds without requiring high-temperature treatments, annealing, or toxic chemical cleaning processes. Instead, a highly accelerated Ar fast atom beam is employed to physically remove contaminants and oxides from the surface of the wafer. Kim et al. [60] proposed a method that used an Ar ion beam on a Cu surface in a UHV environment to eliminate the oxide layer before performing SAB. For successful thermo-compression bonding (TCB), the surface must be free of contaminants and have a flat oxide-free profile. CMP can be used to achieve a root mean square (RMS) surface roughness of 1 nm or less; however, Cu oxidizes quickly, forming an oxide layer over 1 nm thick within just 1 h of environmental exposure [60]. Therefore, the removal of this oxide layer is critical for successful TCB.

In SAB, an ion or high-velocity atomic beam is used to activate the bonding surfaces in a UHV environment, facilitating the formation of chemical bonds between Cu surfaces at room temperature [62]. The SAB setup (as depicted in Fig. 3) consists of various chambers designed for processing, analysis, heating, and alignment. After the surface activation in the process chamber, the two wafers are brought into contact and bonded in the bonding chamber. This enables wafer-level Cu-Cu bonding using an Ar ion beam with SAB technology. The surface activated Cu-Cu bonding process involves specialized treatments that remove or prevent the formation of an oxide layer on the Cu surface. This results in a strong bond at room temperature without needing an annealing step to increase the bond strength. Auger electron spectroscopy (AES) was used to assess the cleanliness of the Cu surfaces prior to bonding. Following the Ar ion beam treatment, the transfer of the Cu sample from the process chamber to the analysis chamber took approximately 15 min, during which

time residual gases like O_2, H_2, and O could be generated. However, Auger analysis confirmed that these gases had a minimal impact on the surface.

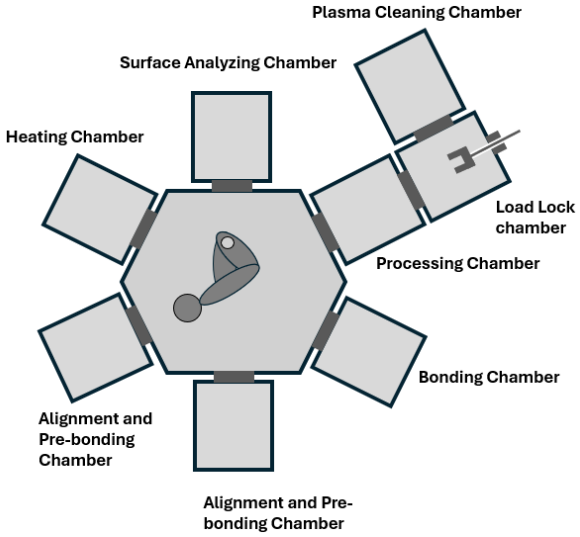

Fig. 3 Schematic view of surface activated bonding machine

The bond strength, a key measure of bonding quality, was assessed, and the tensile strength was found to exceed 6.47 MPa, with fractures occurring in the bulk or glue. This demonstrates that Cu-Cu bonding at room temperature can be successfully achieved using an Ar ion beam during the SAB process. Shigetou et al. [65] demonstrated the successful bonding of 6 μm-pitch bumpless Cu electrodes using the SAB method; their technique also facilitated bonding of 20 μm-pitch Au microbumps at room temperature [66].

3.2. Enhanced Mechanical Bonding Strength by Chemical Pretreatment

The formation of CuO is inevitable during Cu-Cu bonding [67-70], especially at high bonding temperatures. Cu is highly susceptible to oxidation, with an oxide layer over 1 nm thick formed in less than 1 h of exposure [71]. Although several methods have been proposed to remove this oxide layer [72-75], they are primarily limited to wafer-to-wafer bonding, highlighting the need for new techniques. Consequently, various approaches have been explored to remove the oxide layer before bonding.

Exposure of the surface to various contaminants, as well as the oxide film, is not good for bonding quality as it causes voids. So chemical pretreatment of Cu surfaces is employed prior to bonding or film growth to remove native oxides and organic contaminants and to smooth calendering induced roughness. For example, agents such as ammonium persulfate or acetic acid improve surface cleanliness and planarity, thereby promoting uniform nucleation, enlarging effective contact area, and reducing interfacial resistance and voiding. Process conditions must avoid overetching that can introduce pits [76]. Fig. 4 is a scanning electron microscopy (SEM) image showing the differences before and after two chemical pretreatments (AP: ammonium persulfate, AA: acetic acid) on a single slide. The top row

(a–c) shows the surface of the pretreated Cu foil itself, while the bottom row (d–f) shows the graphene surface grown on each Cu foil. As shown in Fig. 4 (a), untreated Cu foil exhibits distinct stripe patterns and poor flatness due to marks from the commercial calendering process. (b) Pretreatment with AP reduces the stripe patterns, significantly improving flatness, but in areas where the oxide layer is not sufficiently dense, the solution directly etches the Cu itself, resulting in small particles/protrusions on the surface. (c) Pretreatment with AA results in milder etching compared to AP, avoiding direct etching of the Cu substrate, thereby achieving better flatness without small protrusions. In summary, surface flatness follows the order of AA treatment > AP treatment > untreated. (d) Graphene grown on untreated Cu shows numerous white spot like impurities, which are interpreted as particles formed by the melting and aggregation of Cu surface oxides during the growth and cooling process. (e) Graphene grown on AP pretreated Cu shows a reduction in the number of white particles, confirming the oxide removal effect, but they are still scattered. (f) Graphene grown on AA pretreated Cu has a very smooth surface with extremely few impurities, making it the cleanest of the three in terms of surface cleanliness.

In summary, Fig. 4 illustrates the effect of pretreatment agents on Cu surface flatness and oxide removal, and how these results directly impact graphene surface cleanliness, as shown intuitively by SEM. AA produces the most uniform and clean Cu/graphene surface, while AP is effective but leaves some overetching and residual particles. Through this study, we can understand why chemical pretreatment is applied to metal surfaces.

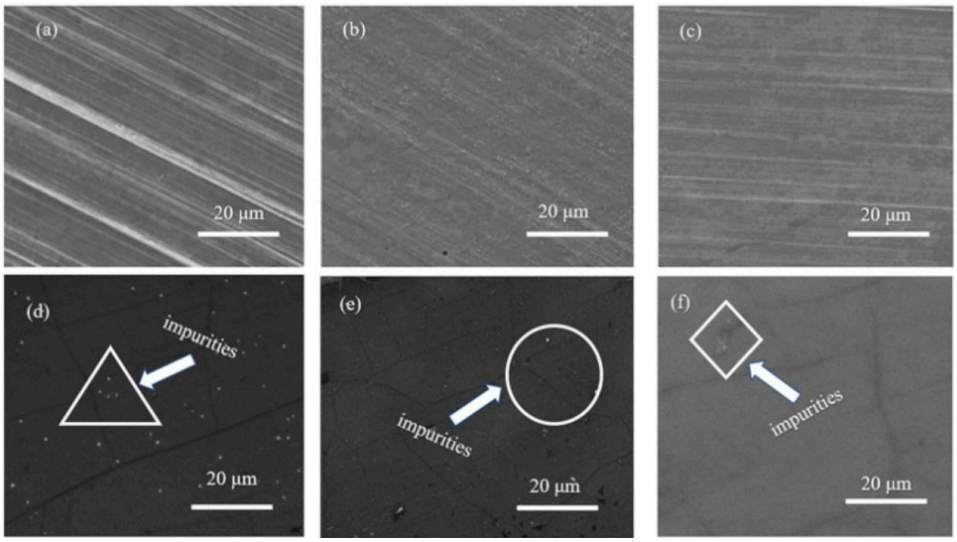

Fig. 4 SEM of (a) pristine copper foil without pre-treatment; (b) copper foil treated with AP solution; (c) copper foil treated with AA solution; (d) graphene grown on pristine copper foil without pre-treatment; (e) graphene grown on copper foil treated with AP solution; (f) graphene grown on copper foil treated with AA solution [76]

Jangam et al. [77] introduced a method that used formic acid to eliminate the oxide layer. Fig. 5 depicts an integrated apparatus that both generates formic acid (HCOOH) vapor and provides a treatment/bonding chamber for Cu films. In this setup, nitrogen is

passed through a reservoir of concentrated formic acid (98% HCOOH) to create a dilute vapor stream, approximately 1% HCOOH in 99% N_2, which is delivered to the chamber designed for surface treatment and subsequent bonding. The Cu sample is mounted on a heated stage; prior to dosing, the chamber is evacuated to ~5 Pa and the sample temperature is raised to 200 °C to establish a low oxygen environment and activate surface chemistry [78]. Once the mixed HCOOH/N_2 stream enters the chamber and impinges on the heated Cu surface, gas phase HCOOH adsorbs and dissociates to form surface formate and hydrogen species; near 200 °C the formate further decomposes to release CO_2 and atomic hydrogen. The generated hydrogen reduces native copper oxides to metallic Cu with evolution of CO_2 and H_2O, thereby restoring a bondable surface. The volatile byproducts are continuously removed through the exhaust, and—using the same apparatus shown in Fig. 5—the treated surfaces are subsequently brought into contact and bonded at 200 °C under load. This technique allowed for localized cleaning, completing the process in less than 10 s, thereby enhancing the overall efficiency. These reactions occurred between 100 and 150 °C, when formic acid reacted with the CuO layer to produce copper formate and vapor. Above 200 °C, copper formate decomposed into CO_2 and H_2 gas, leaving behind pure Cu metal. After the oxide was removed, Cu-Cu bonding was performed at 240 °C for 5 s, resulting in excellent bonding with an average shear strength of over 150 MPa [78].

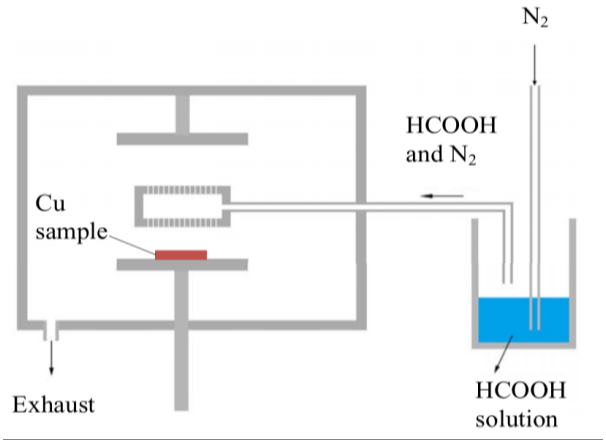

Fig. 5 Schematic of formic acid vapor generation and Cu sample treatment/bonding machine. Reproduced from [78]

In addition to formic acid, other acids such as sulfuric [79], acetic [80], citric [81], hydrochloric [74, 75], and fluorine-containing plasma [65, 82] have been used to remove oxide layers. However, the use of acidic solutions is not always suitable for complementary metal oxide semiconductor (CMOS) devices. In the CMOS industry, acidic solutions are generally avoided because they may negatively affect the device performance and reliability.

3.3. Cu-Cu Mechanical Bonding by Passivation

3.3.1. Pd and Sn Passivation to Enhance Mechanical Reliability of Cu-Cu Bonding

As mentioned earlier, acidic substances such as acetic acid can remove the CuO film, but they also etch the Cu layer, making the removal of the oxide layer difficult to control [80, 83]. To address this issue, many researchers have focused not only on removing the oxide layer from preoxidized Cu surfaces but also on preventing further oxidation [84-87]. The passivation method allows bonding at lower temperatures, eliminating the need for sputtering deposition and vacuum bonding, thereby offering a more efficient and cost-effective solution. However, previous studies that used passivation for research purposes primarily relied on sputtered Cu for bonding [84, 88]. Sputtered films tend to have a lower roughness and higher uniformity than those formed by other deposition techniques. Despite this, Pd passivation stands out because of its stable electrical performance, reliability at low temperatures, and ability to resist corrosion and degradation.

Tsai et al. [89] used Pd passivation to overcome the challenges of Cu oxidation and facilitated Cu-Cu bonding at reduced temperatures. In their approach, a 50 nm Ti layer and 200 nm Cu seed layer were initially deposited onto a Si wafer. A 2 μm photoresist layer was then coated and patterned on the seed layer, followed by electroplating to form the Cu redistribution layer (RDL). After another lithography process to enhance the photoresist, a 10 μm photoresist layer was applied and patterned for Cu pillar micro bumps, and 5 μm high Cu pillars were electroplated. The wafer was then cleaned with dilute sulfuric acid to remove the surface oxides on the Cu pillars, and a 10 nm Pd passivation layer was deposited to prevent reoxidation. The bonding process was carried out at 1.91 MPa and 150 °C for 50 min, with an operating pressure of 7×10^{-3} Torr and base pressure of 1×10^{-6} Torr, without additional surface treatments. The structure with Ti passivation exhibited a noncontact resistance of 7×10^{-4} Ω·cm², while the structure with Pd passivation showed significantly lower resistance at 2×10^{-7} Ω·cm². Reliability tests confirmed that the Pd passivated material offered a high resistance to temperature and humidity degradation [89].

Kung et al. [90] addressed Cu surface oxidation and height nonuniformity by introducing a thin Sn passivation layer atop electroplated Cu and then employing low-temperature, low-pressure thermo-compression to enable direct Cu-Cu bonding without CMP. Sn's low melting point (232 °C) and high deformability allow it to conformally bridge pad-to-pad topography, thereby accommodating surface roughness and pillar height mismatch while promoting intimate metallic contact. The process flow comprised sputtering a 50 nm Ti adhesion layer and a 300 nm Cu seed on Si, electroplating ~5 μm Cu, and depositing Sn at controlled thicknesses of 1 μm, 800 nm, and 600 nm as the principal variable. After acetone and 50 vol% HCl cleans, wafers were bonded in ~10^{-2} torr ambient with a 40 °C min^{-1} ramp, 1 min dwell at the target temperature, and 1–2 MPa applied pressure, followed by N_2 purge cooling. Two temperature windows were emphasized: 220 °C (solid Sn, minimizing collateral reflow risks) and 250 °C (transient liquid assisted flow, maximizing gap fill and planarity compensation).

Fig. 6 (b) establishes the governing defect formation mechanism when Sn is insufficient to fully mediate roughness during intermetallic growth. As Sn is consumed, scalloped Cu_6Sn_5 and smoother Cu_3Sn emerge at the reaction front; if the residual Sn thickness is too small, the opposing intermetallic compound (IMC) surfaces first touch at asperities, concentrating load locally and leaving low pressure regions that preserve micron scale gaps. This "Sn depletion → roughness amplification → stress concentration" pathway explains

the observed transition from isolated microvoids to extended unbonded lines and large voids in thin Sn regimes. Experimentally, 800 nm Sn at 220 °C even under 2 MPa produced large voids attributable to early rough IMC contact, whereas 250 °C promoted more complete IMC formation and improved integrity but remained thickness limited for gap accommodation. At 600 nm Sn, residual micro gaps persisted at both temperatures despite raising pressure to 2 MPa, underscoring the need for a minimum Sn budget to suppress roughness induced defects.

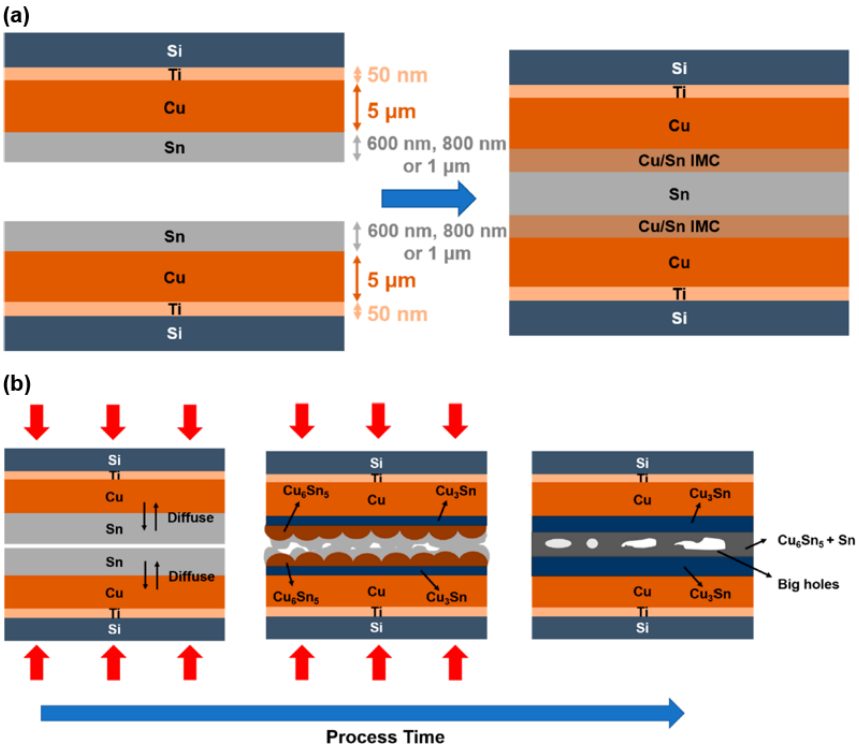

Fig. 6 Schematic of (a) the Cu-to-Cu direct bonding using Sn as the passivation layer and (b) IMC formation and microstructure evolution of the Cu-Sn bonding when Sn is not thick enough

Quantitatively, the most robust condition was 1 μm Sn bonded at 250 °C and 1 MPa, yielding ~0.9% areal void fraction with ~13% unbonded length. Under otherwise comparable settings, 1 μm Sn at 220 °C (1 MPa) and 800 nm at 250 °C (2 MPa) both produced ~1.5% voiding with ~20–25% unbonded length, while the worst case—800 nm Sn at 220 °C and 2 MPa—exhibited ~4.7% voiding and ~37.5% unbonded length due to the large void mechanism highlighted in Fig. 6 (b). Surface planarization strongly mitigated these Fig. 6 (b) type defects: the RMS (R_q) of Cu surface roughness dropped from ~22 nm (as plated) to ~1.3 nm (polish + CMP) and peak-to-valley height variation from ~0.96 μm to ~0.28 μm, driving, for example, the 800 nm/220 °C case from ~4.8% voiding and ~37.3% unbonded length down to ~0.3% and ~7.35%, respectively; 800 nm/250 °C then

met targets even at 1 MPa, and 600 nm/250 °C/2 MPa became acceptable. Cross-sectional transmission electron microscopy (TEM) further supports the microstructural soundness: at 1 μm/250 °C/1 MPa/1 min, a Cu/Cu_6Sn_5/Cu_3Sn/Cu_6Sn_5/Cu stack formed without interfacial flaws; at 800 nm/250 °C/2 MPa, the IMCs converted fully to Cu_3Sn with clean Cu-Cu_3Sn interfaces, consistent with literature reported high shear strengths for Cu/Cu_3Sn/Cu joints [90].

This study demonstrates that transient liquid assisted bonding with ≥1 μm Sn achieves high-quality Cu-Cu interconnects at 250 °C and 1 MPa within 1 min, without CMP. A prudent caveat is that the optimization relies primarily on structural metrics (voiding, unbonded length, TEM); for process window definition in product settings, complementary electrical contact resistance and long-term reliability under coupled thermo-humidity and thermal cycling loads should be quantified under the same conditions.

In summary, the use of Pd and Sn as a passivation layer significantly reduced the contact resistance, resulting in superior electrical properties suitable for interconnect applications. These studies demonstrated that Pd and Sn passivation facilitates high-quality Cu-Cu bonding at low temperatures with stable electrical performance, making it ideal for low-thermal-budget applications in 3D integration.

3.3.2. Au Passivation and Cr/Au Passivation

In addition to Pd passivation, we explored Cu-Cu bonding using Au passivation. The key advantage of Au passivation is that it enables bonding at a lower temperature than Pd passivation, while improving the electrical properties and providing excellent bonding strength in tensile tests. Moreover, Au passivation can be applied directly at both the wafer and chip levels. However, one drawback is the formation of IMCs during bonding, which exhibit poor electrical properties, low structural stability, and require large bump pitches, negatively affecting the bonding process. There are two methods for passivating Ag or Au: one uses sputtering and an e-beam [91], and the other uses a metal capping layer on top of RDL + low-temperature TCB [92, 93].

Liu et al. [92] proposed using Au as a passivation material. They conducted bonding at a low temperature of 150 °C for 30 min under a vacuum of 0.01 Torr through TCB. During bonding, Cu diffused through the Au layer to the bonding interface, forming a strong bond. No IMCs were observed, probably because of the difficulty in nucleation at low temperatures. The mechanical strength was evaluated via a pull test, which revealed a bonding strength of 0.94 MPa, indicating a high-quality bond. The electrical performance was also excellent, with a noncontact resistance of approximately 10^{-8} Ω·cm², regardless of the contact size.

Liu et al. [93] discovered that a Cr wetting layer between the RDL and Au passivation layer reduced the bonding temperature to 70 °C. They found that bonding could be completed in 15 min at 100 °C for wafer-level applications and in 180 s at 70 °C for chip-level applications. AES confirmed the diffusion of Cu atoms from the Cr wetting layer to the bonding surface. For comparison, atomic force microscopy (AFM) was used to measure the RMS surface roughness of various samples, including Cu surfaces with 2 nm Cr and 8 nm Au layers, Cu surfaces with 10 nm Au layers, and Cu RDLs. The RMS values were 3.2 nm for Cu, 2.75 nm for Cu/Au, and 2.55 nm for Cr/Au. These findings demonstrated that the Cr/Au layer resulted in a more uniform surface roughness, thereby improving the bonding quality and minimizing voids. Scanning acoustic tomography and SEM further confirmed the superior bonding quality of the passivated layer, compared with that of the layers without passivation.

A chip pull test was conducted to assess the mechanical strength, and revealed that the bonding strength at the wafer level exceeded the mechanical strength of the adhesive (11.89 MPa), as cracks appeared at the interface between the fixative adhesive and silicon substrate. The success of the chip-level bonding, as a function of temperature and time, is presented in Table 3.

Table 3 Bonding success as a function of temperature and time

	180 s	60 s	30 s	15 s
200 °C	Success	-	-	-
180 °C	-	-	-	Success
150 °C	Success	-	Success	Success
120 °C	Success	Success	Success	Fail
100 °C	-	Success	Fail	-
70 °C	Success	Fail	-	-
60 °C	Fail	-	-	-

Despite the Cr wetting layer, the noncontact resistance increased to approximately 10^{-7} $\Omega \cdot cm^2$ at supply currents ranging from 0 to 100 mA. Additional tests were conducted to assess the mechanical strength of chip-level bonding with Au and Cr/Au passivation layers at 200 and 120 °C, as presented in Table 4.

Table 4 Bonding strength of Au and Cr/Au passivation at 200 °C and 120 °C

Passivation	Parameter (Temperature/Time)	Force (MPa)
Au	200 °C/180 s	4.69
Au	120 °C/180 s	1.19
Cr/Au	200 °C/180 s	5.11
Cr/Au	120 °C/180 s	1.75

As shown in Table 4, the bonding strengths of chips with Cr/Au passivation are superior to those of the chips with Au passivation at both 200 and 120 °C. This demonstrates that Cr wetting and Au passivation can improve the surface roughness, enhance the bonding quality, and ensure strong mechanical performance at both the chip and wafer levels. Thus, we can conclude that Au and Cr/Au passivation not only protects Cu from oxidation prior to bonding at ultralow temperatures but also facilitates Cu diffusion to the bonding surface. In particular, Cr/Au passivation enhances the surface roughness, further improving the bonding quality.

Lee et al. [91] reported a representative example of low-temperature Cu-Cu hybrid bonding enabled by noble-metal passivation nanolayers, specifically Au and Ag, deposited on Cu pads for Cu/SiO_2 hybrid bonding applications. In their process, ~12 nm Au and ~15 nm Ag were formed by e-beam evaporation on 1 μm Cu films, with the nanolayers acting simultaneously as oxidation barriers and diffusion mediators during bonding at 180 °C followed by annealing at 200 °C. Fig. 7 (d) in their work schematically illustrates the heating test used to quantify diffusion between the passivation metal (Au or Ag) and Cu. A Ti adhesion layer is first sputtered on thermally oxidized Si, followed by a 1 μm Cu film, on top of which a nanometer-scale Au or Ag layer is evaporated. This stack is then subjected to isothermal heating at 25, 100, 150, and 200 °C for 1 h, and the evolution of the surface chemistry and depth profile of Au/Ag, Cu, and O is analyzed by X-ray photoelectron

spectroscopy (XPS) and TEM. Through this protocol, Lee et al. [91] extract diffusion activation energies for both Au↔Cu and Ag↔Cu, showing that Au diffuses more readily into Cu than Cu into Au, whereas for Ag–Cu the opposite trend holds. These data position Au and Ag nanolayers as tunable passivation/diffusion layers that enable solid-state interdiffusion at ≤200 °C while maintaining Cu surface protection during the pre-bond steps.

Fig. 7 (d) focuses specifically on the Cu-Cu bonding interface when an Au nanolayer is employed as the passivation layer. SEM and TEM observations reveal a porous Au nanolayer at the bonding interface, with the dark contrast region corresponding to Cu together with oxygen that was introduced prior to bonding, and a bright narrow band associated with Au along the interface. The accompanying energy dispersive spectroscopy (EDS) line scan in Fig. 7 (d) demonstrates a pronounced oxygen peak localized at the Au/Cu interface, indicating that oxygen contamination was already present at the Au–Cu interface before bonding and that the porous morphology of the Au nanolayer allowed limited oxygen ingress without forming bulk intermetallics. Nonetheless, after bonding and annealing, Au is largely diffused into Cu, and the interface is filled predominantly with Cu and O residues rather than a distinct Au layer. From the viewpoint of metal passivation engineering (e.g., Au/Ag/Cr passivation schemes in Cu hybrid bonding), Fig. 7 shows that an ultrathin Au passivation nanolayer can both suppress Cu oxidation sufficiently for low-temperature bonding and participate in controlled interdiffusion, while the porous nature and oxygen uptake at the interface must be carefully managed to optimize mechanical strength and interfacial cleanliness.

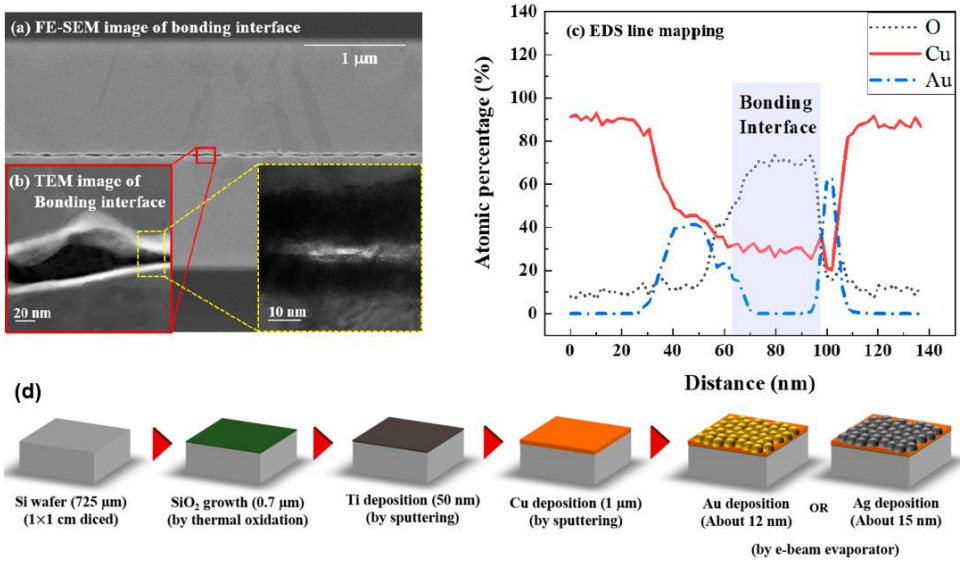

Fig. 7 (a) FE-SEM and (b) TEM analysis results of a bonded wafer using an Ag passivation nanolayer and (c) EDS scanning results and (d) Schematic diagram of Au and Ag passivation on Cu [91]

3.4. Cu-Cu Mechanical Bonding Using Cu (111) Surface of nt-Cu

Several studies have shown that Cu diffusion on the (111) surface is the most favorable for Cu-Cu bonding [94-100]. The development of nt-Cu through electrodeposition facilitates Cu-Cu bonding at temperatures below 250 °C by producing Cu films dominated by (111)-oriented grains, which exhibit the highest surface diffusivity [101].

Table 5 illustrates that the (111) surface has a diffusion coefficient three to four orders of magnitude higher than that of the other orientations. This higher diffusivity allows for lower bonding temperatures on the (111) surface. A (111) orientation for nt-Cu can be achieved through electroplating or sputtering. For example, a 97% (111)-oriented Cu film was fabricated by sequentially sputtering a 100 nm thick Ti adhesion layer and 200 nm thick Cu film onto an 8-inch Si wafer using an Oerlikon Cluster Line 300. However, the large-scale production of (111)-oriented Cu remains challenging. To address this issue, the (111)-oriented single-crystal Cu surface can be replaced with a highly (111)-oriented polycrystalline Cu thin film.

Table 5 Calculated Cu surface diffusivity on (111), (100), and (110) planes at various temperatures ranging from 150 to 300 °C

D_{surf} / Temp. (cm^2/s)	(111)	(100)	(110)
300 °C	1.51×10^{-5}	1.48×10^{-8}	1.55×10^{-9}
250 °C	1.22×10^{-5}	4.74×10^{-9}	3.56×10^{-10}
200 °C	9.42×10^{-6}	1.19×10^{-9}	5.98×10^{-11}
150 °C	6.85×10^{-6}	2.15×10^{-10}	6.61×10^{-12}

For successful direct Cu-Cu bonding, at least one surface must be (111) oriented. The bonding proceeds more efficiently if both Cu surfaces are aligned along the <111> axis [101]. Researchers have bonded nt-Cu pieces to randomly oriented Cu pieces at different temperatures to study void formation. Bonding at 150 °C for 1 h results in voids, but void formation is significantly reduced at 200 °C for 30 min or 250 °C for 10 min. EBSD was used to confirm the orientations of the bonded materials. The tensile strengths of five 2×2 cm^2 samples of 97% (111)-oriented Cu films bonded at 200 °C for 1 h were tested. Three of the five samples demonstrated tensile strengths above 4.3 MPa, while the remaining two showed fracture strengths of 2.7 and 1.3 MPa, confirming good tensile strength.

Shie et al. [102] reported that Cu-Cu bonding can be achieved at 300 °C in only 10 s by employing nt-Cu with a <111> orientation. The nt-Cu microstructure provides both excellent mechanical properties and strong resistance to electromigration. In their study, 30-μm-diameter nt-Cu bumps were electrodeposited on 8-inch wafers, planarized by CMP to a surface roughness of Rq ≈ 5 nm, and de-oxidized in a citric-acid solution for 30 s, followed by chip-to-chip bonding in N_2 at 300 °C under an applied pressure of approximately 90 MPa. Under these conditions, the bonding interface after a 10 s process was nearly void-free; most of the (111)-oriented nt-Cu grains were preserved, and only limited detwinning was observed near the passivation openings. Single-joint resistance measurements using Kelvin structures yielded low values of approximately 4.4–4.9 mΩ with only weak dependence on bonding time in the range of 10–60 s. These findings indicate that the high surface diffusivity of Cu (111) at 300 °C plays a dominant role in enabling rapid bonding and that reliable Cu-Cu joints can be realized even when the (111)-oriented surface fraction of the bumps is as low as about 40%.

Lu et al. [103] fabricated approximately 6 μm-thick nt-Cu films with a strong (111) texture by electroplating on a (111)-oriented Cu seed layer followed by CMP, and then introduced an epoxy-induced surface modification to obtain an epoxy-treated nanotwinned Cu (Ent-Cu) structure. As shown in Fig. 8, EBSD and grain-size analyses indicate that the as-deposited nt-Cu exhibits a columnar nanotwinned microstructure with a highly (111)-oriented surface, whereas after repeated thermal cycling in contact with an epoxy the Ent-Cu develops a dual-layer structure in which the top ~1 μm is transformed into a fine-grained, randomly oriented layer with an average grain size of about 0.2 μm, while the underlying nt-Cu retains its strong (111) texture.

Using these films for Cu-Cu TCB in the temperature range of 200–300 °C, Lu et al. [103] found that in the conventional nt-Cu joints the bonding interface remains largely intact even at 300 °C, as evidenced in Fig. 8 (a), where only a mildly zigzagged but still distinct boundary is observed with limited grain penetration across the interface.

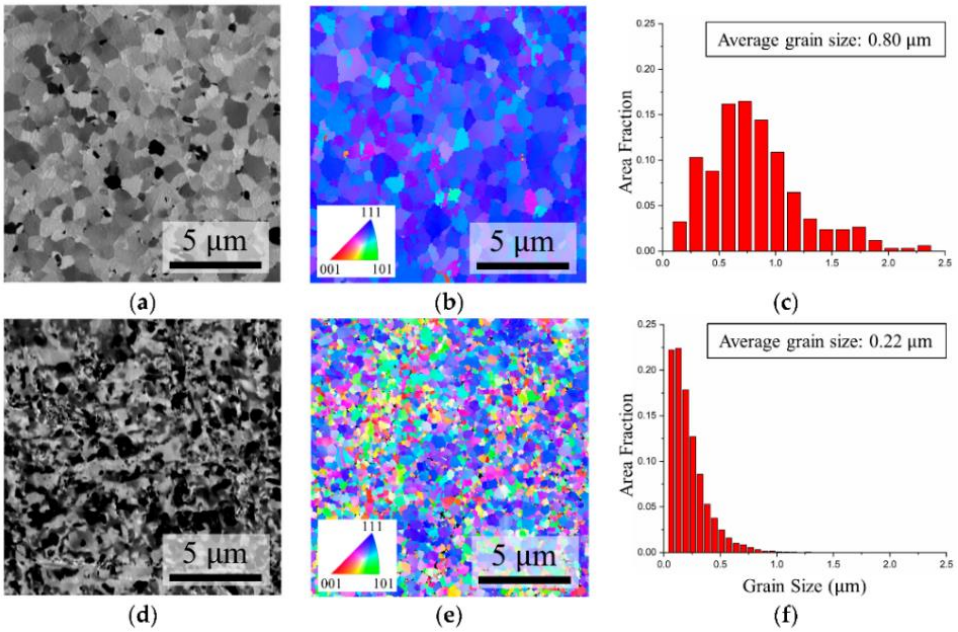

Fig. 8 Microstructures of initial Cu films. (a) Plane-view scanning ion microscopy (SIM) image of nt-Cu. (b) Plane-view EBSD OIM image of nt-Cu. (c) Distribution of grain sizes for the grains in (b). (d) Plane-view SIM image of Ent-Cu. (e) Plane-view EBSD OIM image of Ent-Cu. (f) Distribution of grain sizes for the grains in (e) [103]

In contrast, the Ent-Cu joints exhibit pronounced abnormal grain growth originating from the fine-grained interfacial layer; Fig. 9 (b) demonstrates that large grains extend into both Cu films and effectively consume the original Cu-Cu interface, leading to an almost interface-free microstructure after bonding at 300 °C. These observations imply that merely exposing a fully (111)-oriented nt-Cu surface is insufficient for interface elimination, and that only when a highly defective, high grain-boundary-energy fine-grained surface layer is introduced on top of a (111)-textured nanotwinned underlayer, as characterized in Fig.

9, can the interface-free Cu-Cu joint structure observed in Fig. 9 be achieved at relatively low temperatures. The (111)-based Cu-Cu bonding route demonstrated by Lu et al. [103] therefore offers the advantage of maintaining a reliable (111)-oriented nt-Cu backbone for current conduction while eliminating the bonding interface without noble-metal interlayers, but it also suffers from the requirement of a still relatively high bonding temperature around 300 °C, increased process complexity due to epoxy thermal cycling and additional CMP, and partial loss of the (111) texture at the immediate bonding surface.

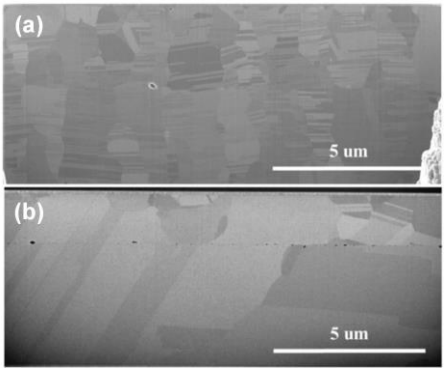

Fig. 9 Cross-sectional SEM images after bonding at 300 °C for 1 h: (a) nt-Cu; (b) Ent-Cu [103]

4. CONCLUSION

This review explored the various factors influencing Cu-Cu mechanical bonding and provided a detailed analysis of the fundamental principles governing these effects. The key parameters affecting Cu-Cu bonding were identified as the thickness of the bonding layer, grain size, temperature, and surface roughness. Increasing the Cu thickness was found to enhance the bonding energy because of changes in the surface microstructure that depend on the thickness; these changes were examined in detail by introducing artificial voids and performing subsequent theoretical analyses. In addition, grain refinement was shown to suppress microcrack formation and propagation, thereby improving the bonding performance, while higher bonding and annealing temperatures promoted atomic diffusion and accelerated bond formation. With regard to surface roughness, the bonding quality improved as the roughness decreased and the true contact area increased, but beyond a critical condition void formation degraded the bonding strength. Various methods for achieving low-temperature bonding, such as SAB, passivation, and chemical pretreatment, have been widely studied to improve the Cu-Cu bonding quality, and the advantages, disadvantages, and characteristics of these techniques are summarized in Table 6.

At the same time, the high oxidation tendency of Cu continues to impose severe constraints on the available thermal budget, giving rise to issues such as wafer deformation, increased integration complexity, and limited compatibility with front end device structures. Future progress toward more reliable and manufacturable Cu-Cu joints will therefore depend on the combined optimization of microstructure design (including grain size, preferred orientation, and thickness), surface engineering (including roughness and oxide control), and thermo-mechanical loading paths, particularly under low-temperature and

fine-pitch conditions. In addition, practical implementation in high-throughput 3D integration will require chemistries that are compatible with CMOS processing, scalable Cu architectures dominated by the (111) orientation or based on nanocrystalline Cu, and robust inline metrology and defect screening schemes for interfacial voids and failures related to surface roughness. The continued development of such Cu-Cu bonding strategies under a low thermal budget is essential to fully exploit ultra-high-density interconnects in next-generation three-dimensional integration, where very high input and output density, power efficiency, and long-term reliability must be satisfied at the same time.

Table 6 Comparison of Cu-Cu bonding methods

Bonding method	Bonding temperature	Advantages	Disadvantages	Reference
SAB	200 °C -250 °C	High bonding quality without toxic chemical cleaning	UHV environment Low throughput Complex process	[60-64]
Chemical pretreatment	250 °C -300 °C	Low cost	Only wafer–wafer bonding Low bonding quality	[65, 74, 75, 77, 80-82]
Pd passivation	150 °C	High bonding quality, High electrical performance and reliability	Limited application Hard to control surface roughness	[89]
Au, Cr/Au passivation	120 °C	Very low bonding temperature, High electrical performance High reliability	IMC formation	[92, 93]
(111) oriented nt-Cu	150 °C -300 °C	High CMOS compatibility	Limitation of fine-pitch Cu bump structure	[101, 102]

Acknowledgement: *This research was supported by GRDC (Global Research Development Center) Cooperative Hub Program through the National Research Foundation of Korea (NRF) funded by the Ministry of Science and ICT (MSIT) (RS-2023-00257595).*

REFERENCES

1. Zhao, G., Song, C., Wu, B., 2024, *3D integrated circuit (3D IC) technology and its applications*, Journal of Industrial Engineering and Applied Science, 2(4), pp. 60-65.
2. Agarwal, R., Cheng, P., Shah, P., Wilkerson, B., Swaminathan, R., Wuu, J., Mandalapu, C., 2022, *3D packaging for heterogeneous integration*, Proc. 2022 IEEE 72nd Electronic Components and Technology Conference (ECTC), San Diego, USA, pp. 1103-1107.
3. Lee, S., Jee, Y., Park, S., Lee, S., Hwang, B., Jo, G., Lee, C., Park, J., Jang, A., Jung, H., Kim, I., Kang, D., Baek, S., Kim, D.W., Kang, U., 2022, *A study on memory stack process by hybrid copper bonding (HCB) technology*, Proc. 2022 IEEE 72nd Electronic Components and Technology Conference (ECTC), San Diego, USA, pp. 1085-1089.
4. Light, D., Faraci, A., Fjelstad, J., 1998, *Chip-size package technology for semiconductors*, Microwave Journal, 41(5), pp. 280-288.

5. Chen, K.N., Tan, C.S., 2011, *Integration schemes and enabling technologies for three-dimensional integrated circuits*, IET Computers and Digital Techniques, 5(3), pp. 160-168.
6. Ni, T., Yang, Z., Chang, H., Zhang, X., Lu, L., Yan, A., Huang, Z., Wen, X., 2021, *A novel TDMA-based fault tolerance technique for the TSVs in 3D-ICs using honeycomb topology*, IEEE Transactions on Emerging Topics in Computing, 9(2), pp. 724-734.
7. Koester, S., Young, A., Yu, R., Purushothaman, S., Chen, K.-N., La Tulipe, D., Narender, R., Shi, L., Wordeman, M., Sprogis, E., 2008, *Wafer-level 3D integration technology*, IBM Journal of Research and Development, 52(6), pp. 583-597.
8. Peng, L., Li, H., Lim, D., Gao, S., Tan, C., 2011, *High-density 3-D interconnect of Cu–Cu contacts with enhanced contact resistance by self-assembled monolayer (SAM) passivation*, IEEE Transactions on Electron Devices, 58(8), pp. 2500-2506.
9. Bae, J.Y., Kim, M.-S., Lee, H.M., Lee, S.G., Lee, Y.-W., Moon, J.T., Hong, W.S., 2023, *Bonding property of middle temperature Sn-Ag-Cu solder ball joint of ball grid array package*, Journal of Welding and Joining, 41(5), pp. 379-386.
10. Zhang, S., Kim, S.-H., Kim, T.-W., Kim, Y.-S., Paik, K.-W., 2014, *A study on the solder ball size and content effects of solder ACFs for flex-on-board assembly applications using ultrasonic bonding*, IEEE Transactions on Components, Packaging and Manufacturing Technology, 5(1), pp. 9-14.
11. Noguchi, K., Ikeda, M., Shimizu, I., Kawamura, Y., Ohno, Y., 2001, *Effect of cooling rate on microstructure and strength properties of tin-silver-copper solder ball bonding*, Materials Transactions, 42(5), pp. 761-768.
12. Hua Zhong, C., Yi, S., 1999, *Solder joint reliability of plastic ball grid array packages*, Soldering and Surface Mount Technology, 11(1), pp. 44-48.
13. Kim, J.-W., Kim, D.-G., Jung, S.-B., 2005, *Mechanical strength test method for solder ball joint in BGA package*, Metals and Materials International, 11(2), pp. 121-129.
14. Lee, T.-K., Ma, H., Liu, K.-C., Xue, J., 2010, *Impact of isothermal aging on long-term reliability of fine-pitch ball grid array packages with Sn-Ag-Cu solder interconnects: surface finish effects*, Journal of Electronic Materials, 39(10), pp. 2564-2573.
15. Lee, C.-B., Jung, S.-B., Shin, Y.-E., Shur, C.-C., 2002, *Effect of isothermal aging on ball shear strength in BGA joints with Sn-3.5 Ag-0.75 Cu solder*, Materials Transactions, 43(8), pp. 1858-1863.
16. Lee, T.-K., Zhou, B., Blair, L., Liu, K.-C., Bieler, T.R., 2010, *Sn-Ag-Cu solder joint microstructure and orientation evolution as a function of position and thermal cycles in ball grid arrays using orientation imaging microscopy*, Journal of Electronic Materials, 39, pp. 2588-2597.
17. Gain, A.K., Chan, Y.C., Yung, W.K., 2009, *Effect of nano Ni additions on the structure and properties of Sn–9Zn and Sn–Zn–3Bi solders in Au/Ni/Cu ball grid array packages*, Materials Science and Engineering: B, 162(2), pp. 92-98.
18. Tsukamoto, H., Nishimura, T., Suenaga, S., McDonald, S.D., Sweatman, K.W., Nogita, K., 2011, *The influence of solder composition on the impact strength of lead-free solder ball grid array joints*, Microelectronics Reliability, 51(3), pp. 657-667.
19. Liu, D., Chen, P.-C., Liu, Y.-W., Hu, H.-W., Chen, K.-N., 2021, *Low-temperature (70° C) Cu-to-Cu direct bonding by capping metal layers*, IEEE Electron Device Letters, 42(10), pp. 1524-1527.
20. Wang, P.J., Lee, C.C., 2009, *Silver joints between silicon chips and copper substrates made by direct bonding at low temperature*, IEEE Transactions on Components and Packaging Technologies, 33(1), pp. 10-15.
21. Wang, P.J., Kim, J.S., Lee, C.C., 2008, *Direct silver to copper bonding process,* Journal of Electronic Packaging, 130(4), 045001.
22. Wu, J., Lee, C.C., 2019, *Low-temperature Ag-Ag direct bonding technology for advanced chip-package interconnection*, Proc. 2019 IEEE 69th Electronic Components and Technology Conference (ECTC), Las Vegas, USA, pp. 2302-2308.
23. Fang, J.-P., Cai, J., Wang, Q., Zheng, K., Zhou, Y.-K., Geng, Z.-T., 2022, *Low-temperature Au-Au bonding using Ag nanoparticles as intermediate for die attachment in power device packaging*, Applied Surface Science, 593, 153436.
24. Wu, J., Huo, Y., Lee, C.C., 2018, D*irect Ag-Ag bonding by in situ reduction of surface oxides for advanced chip-package interconnection*, Materialia, 4, pp. 417-422.
25. Karimi, M., Tomkowski, T., Vidali, G., Biham, O., 1995, *Diffusion of Cu on Cu surfaces*, Physical Review B, 52(7), pp. 5364-5374.
26. Sørensen, M.R., Mishin, Y., Voter, A.F., 2000, *Diffusion mechanisms in Cu grain boundaries*, Physical Review B, 62(6), pp. 3658-3673.
27. Bai, X.-M., Vernon, L.J., Hoagland, R.G., Voter, A.F., Nastasi, M., Uberuaga, B.P., 2012, *Role of atomic structure on grain boundary-defect interactions in Cu*, Physical Review B—Condensed Matter and Materials Physics, 85(21), 214103.

28. Peng, L., Lim, D., Zhang, L., Li, H., Tan, C.S., 2012, *Effect of prebonding anneal on the microstructure evolution and Cu–Cu diffusion bonding quality for three-dimensional integration*, Journal of Electronic Materials, 41, pp. 2567-2572.
29. Utsumi, J., Ichiyanagi, Y., 2014, *Effect of bonding pressure on the strength of Cu/Cu direct bonding by surface activated method*, IEEJ Transactions on Sensors and Micromachines, 134(9), pp. 284-289.
30. Takagi, H., Maeda, R., Chung, T.R., Hosoda, N., Suga, T., 1998, *Effect of surface roughness on room-temperature wafer bonding by Ar beam surface activation*, Japanese Journal of Applied Physics, 37(7), pp. 4197-4203.
31. Gondcharton, P., Imbert, B., Benaissa, L., Verdier, M., 2015, *Copper-copper direct bonding: impact of grain size*, Proc. 2015 IEEE International Interconnect Technology Conference and 2015 IEEE Materials for Advanced Metallization Conference (IITC/MAM), Grenoble, France, pp. 229-232.
32. Timoshevskii, V., Ke, Y., Guo, H., Gall, D., 2008, *The influence of surface roughness on electrical conductance of thin Cu films: an ab initio study*, Journal of Applied Physics, 103(11), 113705.
33. Ke, Y., Zahid, F., Timoshevskii, V., Xia, K., Gall, D., Guo, H., 2009, *Resistivity of thin Cu films with surface roughness*, Physical Review B—Condensed Matter and Materials Physics, 79(15), 155406.
34. Zuo, Y., Shen, J., Xie, J., Xiang, L., 2018, *Influence of Cu micro/nano-particles mixture and surface roughness on the shear strength of Cu-Cu joints*, Journal of Materials Processing Technology, 257, pp. 250-256.
35. Chen, S., Ke, F., Zhou, M., Bai, Y., 2007, *Atomistic investigation of the effects of temperature and surface roughness on diffusion bonding between Cu and Al*, Acta Materialia, 55(9), pp. 3169-3175.
36. Tian, Y., Gao, S., Zhao, L., Lu, S., Pippan, R., Zhang, Z., Tsuji, N., 2018, *Remarkable transitions of yield behavior and Lüders deformation in pure Cu by changing grain sizes*, Scripta Materialia, 142, pp. 88-91.
37. Murakami, M., Moriyama, M., Tsukimoto, S., Ito, K., 2005, *Grain growth mechanism of Cu thin films*, Materials Transactions, 46(7), pp. 1737-1740.
38. Jhan, J.-J., Wataya, K., Nishikawa, H., Chen, C.-M., 2022, *Electrodeposition of nanocrystalline Cu for Cu-Cu direct bonding*, Journal of the Taiwan Institute of Chemical Engineers, 132, 104127.
39. Rebhan, B., Hingerl, K., 2015, *Physical mechanisms of copper-copper wafer bonding*, Journal of Applied Physics, 118(13), 135301.
40. Nieh, T., Wadsworth, J., 1991, *Hall-Petch relation in nanocrystalline solids*, Scripta Metallurgica et Materialia, 25(4), pp. 955-958.
41. Kao, Y.-J., Li, Y.-J., Shen, Y.-A., Chen, C.-M., 2023, *Significant Hall–Petch effect in micro-nanocrystalline electroplated copper controlled by SPS concentration*, Scientific Reports, 13(1), 428.
42. Somekawa, H., Watanabe, H., Higashi, K., 2003, *The grain size dependence on diffusion bonding behavior in superplastic Mg alloys*, Materials Transactions, 44(4), pp. 496-503.
43. Kamiya, S., Shishido, N., Watanabe, S., Sato, H., Koiwa, K., Omiya, M., Nishida, M., Suzuki, T., Nakamura, T., Nokuo, T., 2013, *Grain-scale adhesion strength mapping of copper wiring structures in integrated circuits*, Surface and Coatings Technology, 215, pp. 280-284.
44. Gui, C., Elwenspoek, M., Tas, N., Gardeniers, J.G., 1999, *The effect of surface roughness on direct wafer bonding*, Journal of Applied Physics, 85(10), pp. 7448-7454.
45. Budhe, S., Ghumatkar, A., Birajdar, N., Banea, M., 2015, *Effect of surface roughness using different adherend materials on the adhesive bond strength*, Applied Adhesion Science, 3, 20.
46. Shigetou, A., Itoh, T., Suga, T., 2005, *Direct bonding of CMP-Cu films by surface activated bonding (SAB) method*, Journal of Materials Science, 40(12), pp. 3149-3154.
47. Fick, A., 1855, *On liquid diffusion*, The London, Edinburgh, and Dublin Philosophical Magazine and Journal of Science, 10(63), pp. 30-39.
48. Jang, E.-J., Kim, J.-W., Kim, B., Matthias, T., Park, Y.-B., 2011, *Annealing temperature effect on the Cu-Cu bonding energy for 3D-IC integration*, Metals and Materials International, 17(1), pp. 105-109.
49. Jang, E.-J., Pfeiffer, S., Kim, B.-O., Matthias, T., Hyun, S.-M., Lee, H.-J., Park, Y.-B., 2008, *Effect of post-annealing conditions on interfacial adhesion energy of Cu-Cu bonding for 3-D IC integration*, Korean Journal of Materials Research, 18(4), pp. 204-209.
50. Chiang, P.-H., Liang, S.-Y., Song, J.-M., Huang, S.-K., Chiu, Y.-T., Hung, C.-P., 2017, *Enhanced Cu-to-Cu direct bonding by controlling surface physical properties*, Japanese Journal of Applied Physics, 56(3), 035503.
51. Lin, P.-F., Tran, D.-P., Liu, H.-C., Li, Y.-Y., Chen, C., 2022, *Interfacial characterization of low-temperature Cu-to-Cu direct bonding with chemical mechanical planarized nanotwinned Cu films*, Materials, 15(3), 937.
52. Li, J., Cheng, C., Shi, T., Fan, J., Yu, X., Cheng, S., Liao, G., Tang, Z., 2016, *Surface effect induced Cu-Cu bonding by Cu nanosolder paste*, Materials Letters, 184(5), pp. 193-196.
53. Park, C., Yang, D.-Y., 1996, *A study of void crushing in large forgings I: bonding mechanism and estimation model for bonding efficiency*, Journal of Materials Processing Technology, 57(1-2), pp. 129-140.
54. Kim, H., Kim, J., Kim, Y., Seo, S.-K., Jo, C., Kim, D.-W., 2022, *Process and design optimization for hybrid Cu bonding void*, Proc. 2022 IEEE 72nd Electronic Components and Technology Conference (ECTC), San Diego, USA, pp. 194-197.

55. Cao, T.-S., Mazière, M., Danas, K., Besson, J., 2015, *A model for ductile damage prediction at low stress triaxialities incorporating void shape change and void rotation*, International Journal of Solids and Structures, 63(3), pp. 240-263.
56. Zhang, C., Li, H., Li, M., 2016, *Detailed evolution mechanism of interfacial void morphology in diffusion bonding*, Journal of Materials Science and Technology, 32(3), pp. 259-264.
57. Oh, S.-H., Lee, H.-D., Lee, J.-U., Park, S.-H., Cho, W.-S., Park, Y.-J., Haag, A., Watanabe, S., Arnold, M., Lee, H.-J., 2024, *Thermodynamic modeling framework with experimental investigation of the large-scale bonded area and local void in Cu-Cu bonding interface for advanced semiconductor packaging*, International Journal of Plasticity, 180, 104073.
58. Gao, X., Wang, T., Kim, J., 2005, *On ductile fracture initiation toughness: effects of void volume fraction, void shape and void distribution*, International Journal of Solids and Structures, 42(18-19), pp. 5097-5117.
59. Pardoen, T., Hutchinson, J., 2003, *Micromechanics-based model for trends in toughness of ductile metals*, Acta Materialia, 51(1), pp. 133-148.
60. Kim, T., Howlader, M., Itoh, T., Suga, T., 2003, *Room temperature Cu-Cu direct bonding using surface activated bonding method*, Journal of Vacuum Science and Technology A: Vacuum, Surfaces, and Films, 21(2), pp. 449-453.
61. Shigetou, A., Itoh, T., Suga, T., 2006, *Bumpless interconnect of ultrafine Cu electrodes by surface activated bonding (SAB) method*, Electronics and Communications in Japan (Part II: Electronics), 89(12), pp. 34-42.
62. Taniyama, S., Wang, Y.-H., Fujino, M., Suga, T., 2008, *Room temperature wafer bonding using surface activated bonding method*, Proc. 2008 IEEE 9th VLSI Packaging Workshop of Japan, Tokyo, Japan, pp. 141-144.
63. Liu, H.C., Gusak, A.M., Tu, K.N., Chen, C., 2021, *Interfacial void ripening in Cu–Cu joints*, Materials Characterization, 181, 111459.
64. Wang, Y., Huang, Y.T., Liu, Y.X., Feng, S.P., Huang, M.X., 2022, *Thermal instability of nanocrystalline Cu enables Cu-Cu direct bonding in interconnects at low temperature*, Scripta Materialia, 220, 114900.
65. Shigetou, A., Itoh, T., Sawada, K., Suga, T., 2008, *Bumpless interconnect of 6-μm-pitch Cu electrodes at room temperature*, IEEE Transactions on Advanced Packaging, 31(3), pp. 473-478.
66. Wang, Y.-H., Suga, T., 2008, *20-μm-pitch Au micro-bump interconnection at room temperature in ambient air*, Proc. 2008 58th Electronic Components and Technology Conference, Lake Buena Vista, USA, pp. 944-949.
67. Barr, T., 1977, *ESCA studies of naturally passivated metal foils*, Journal of Vacuum Science and Technology, 14(1), pp. 660-665.
68. Iijima, J., Lim, J.-W., Hong, S.-H., Suzuki, S., Mimura, K., Isshiki, M., 2006, *Native oxidation of ultra high purity Cu bulk and thin films*, Applied Surface Science, 253(5), pp. 2825-2829.
69. Platzman, I., Brener, R., Haick, H., Tannenbaum, R., 2008, *Oxidation of polycrystalline copper thin films at ambient conditions*, The Journal of Physical Chemistry C, 112(4), pp. 1101-1108.
70. Li, J., Vizkelethy, G., Revesz, P., Mayer, J., Tu, K.-N., 1991, *Oxidation and reduction of copper oxide thin films*, Journal of Applied Physics, 69(2), pp. 1020-1029.
71. Badillo-Avila, M., Castanedo-Perez, R., Marquez-Marin, J., Guzman-Caballero, D., Torres-Delgado, G., 2019, *Fast rate oxidation to Cu2O at room temperature of metallic copper films produced by the argon-plasma bombardment of CuO films*, Materials Chemistry and Physics, 236, 121759.
72. Rebhan, B., Plach, T., Tollabimazraehno, S., Dragoi, V., Kawano, M., 2014, *Cu-Cu wafer bonding: an enabling technology for three-dimensional integration*, Proc. 2014 International Conference on Electronics Packaging (ICEP), Toyama, Japan, pp. 475-479.
73. Kang, S.-G., Lee, J.-E., Kim, E.-S., Lim, N.-E., Kim, S.-H., Kim, S.-D., Kim, S.E.-K., 2012, *Fabrication and challenges of Cu-to-Cu wafer bonding*, Journal of the Microelectronics and Packaging Society, 19(2), pp. 29-33.
74. Chen, K.-N., Tan, C., Fan, A., Reif, R., 2005, *Copper bonded layers analysis and effects of copper surface conditions on bonding quality for three-dimensional integration*, Journal of Electronic Materials, 34(3), pp. 1464-1467.
75. Chen, K.-N., Fan, A., Tan, C., Reif, R., 2006, *Bonding parameters of blanket copper wafer bonding,* Journal of Electronic Materials, 35(2), pp. 230-234.
76. Cui, N., Wang, F., Ding, H., 2020, *Acetic acid and ammonium persulfate pre-treated copper foil for the improvement of graphene quality, sensitivity and specificity of Hall effect label-free DNA hybridization detection*, Materials, 13(7), 1784.
77. Jangam, S., Bajwa, A.A., Mogera, U., Ambhore, P., Colosimo, T., Chylak, B., Iyer, S., *2019, Fine-pitch (≤ 10 μm) direct Cu-Cu interconnects using in situ formic acid vapor treatment*, Proc. 2019 IEEE 69th Electronic Components and Technology Conference (ECTC), Las Vegas, USA, pp. 620-627.
78. Yang, W., Lu, Y., Zhou, C., Zhang, J., Suga, T., 2017, *Study of Cu film surface treatment using formic acid vapor/solution for low temperature bonding*, Journal of The Electrochemical Society, 165(4), H3080.
79. Huffman, A., Lannon, J., Lueck, M., Gregory, C., Temple, D., 2009, *Fabrication and characterization of metal-to-metal interconnect structures for 3-D integration*, Journal of Instrumentation, 4(03), P03006.
80. Jang, E.-J., Hyun, S., Lee, H.-J., Park, Y.-B., 2009, *Effect of wet pretreatment on interfacial adhesion energy of Cu-Cu thermocompression bond for 3D IC packages*, Journal of Electronic Materials, 38(7), pp. 2449-2454.

81. Swinnen, B., Ruythooren, W., De Moor, P., Bogaerts, L., Carbonell, L., De Munck, K., Eyckens, B., Stoukatch, S., Tezcan, D.S., Tokei, Z., 2006, *3D integration by Cu-Cu thermo-compression bonding of extremely thinned bulk-Si die containing 10 µm pitch through-Si vias*, Proc. 2006 International Electron Devices Meeting, San Francisco, USA, pp. 71-74.
82. Wang, C., Suga, T., 2010, *A novel room-temperature wafer direct bonding method by fluorine containing plasma activation*, Proc. 2010 60th Electronic Components and Technology Conference (ECTC), Las Vegas, USA, pp. 303-308.
83. Suga, T., 2006, *Cu-Cu room temperature bonding – current status of surface activated bonding (SAB)*, ECS Transactions, 3(6), pp. 155-163.
84. Hong, Z.-J., Liu, D., Hu, H.-W., Cho, C.-I., Weng, M.-W., Liu, J.-H., Chen, K.-N., 2022, *Investigation of bonding mechanism for low-temperature Cu-Cu bonding with passivation layer*, Applied Surface Science, 592, 153243.
85. Tan, C.S., Lim, D.F., Singh, S.G., Goulet, S., Bergkvist, M., 2009, *Cu-Cu diffusion bonding enhancement at low temperature by surface passivation using self-assembled monolayer of alkane-thiol*, Applied Physics Letters, 95(19), 192108.
86. Chou, T.-C., Huang, S.-Y., Chen, P.-J., Hu, H.-W., Liu, D., Chang, C.-W., Ni, T.-H., Chen, C.-J., Lin, Y.-M., Chang, T.-C., 2020, *Electrical and reliability investigation of Cu-to-Cu bonding with silver passivation layer in 3-D integration*, IEEE Transactions on Components, Packaging and Manufacturing Technology, 11(1), pp. 36-42.
87. Panigrahi, A.K., Bonam, S., Ghosh, T., Singh, S.G., Vanjari, S.R.K., 2016, *Ultra-thin Ti passivation mediated breakthrough in high quality Cu-Cu bonding at low temperature and pressure*, Materials Letters, 169(1), pp. 269-272.
88. Lykova, M., Panchenko, I., Künzelmann, U., Reif, J., Geidel, M., Wolf, M.J., Lang, K.-D., 2018, *Characterisation of Cu/Cu bonding using self-assembled monolayer*, Soldering and Surface Mount Technology, 30(2), pp. 106-111.
89. Tsai, Y.-C., Hu, H.-W., Chen, K.-N., 2020, *Low temperature copper-copper bonding of non-planarized copper pillar with passivation*, IEEE Electron Device Letters, 41(8), pp. 1229-1232.
90. Kung, P.-Y., Huang, W.-L., Kao, C.-L., Lin, Y.-S., Hung, Y.-C., Kao, C.R., 2022, *Investigation of low-pressure Sn-passivated Cu-to-Cu direct bonding in 3D integration*, Materials, 15(21), 7783.
91. Lee, S., Park, S., Kim, S.E., 2023, *Low-temperature diffusion of Au and Ag nanolayers for Cu bonding*, Applied Sciences, 14(1), 147.
92. Liu, D., Chen, P.-C., Tsai, Y.-C., Chen, K.-N., 2019, *Low temperature Cu-to-Cu direct bonding below 150 °C with Au passivation layer*, Proc. 2019 International 3D Systems Integration Conference (3DIC), Sendai, Japan, 9058873.
93. Liu, D., Chen, P.-C., Chen, K.-N., 2020, *A novel low-temperature Cu-Cu direct bonding with Cr wetting layer and Au passivation layer*, Proc. 2020 IEEE 70th Electronic Components and Technology Conference (ECTC), Orlando, USA, pp. 1322-1327.
94. Lu, L., Shen, Y., Chen, X., Qian, L., Lu, K., 2004, *Ultrahigh strength and high electrical conductivity in copper*, Science, 304(5669), pp. 422-426.
95. Juang, J.-Y., Lu, C.-L., Chen, K.-J., Chen, C.-C.A., Hsu, P.-N., Chen, C., Tu, K.-N., 2018, *Copper-to-copper direct bonding on highly (111)-oriented nanotwinned copper in no-vacuum ambient*, Scientific Reports, 8, 13910.
96. Liu, C.-M., Lin, H.-W., Lu, C.-L., Chen, C., 2014, *Effect of grain orientations of Cu seed layers on the growth of <111>-oriented nanotwinned Cu*, Scientific Reports, 4, 6123.
97. Li, Y.-J., Tu, K.-N., Chen, C., 2020, *Tensile properties of <111>-oriented nanotwinned Cu with different columnar grain structures*, Materials, 13(6), 1310.
98. Tseng, H.-H., Liu, H.-C., Yu, M.-H., Ong, J.-J., Tran, D.-P., Chen, C., 2023, *Epitaxial growth of (111) nanotwinned Ag on (111) nanotwinned Cu films for low-temperature Cu-Cu bonding*, Crystal Growth and Design, 23(8), pp. 5519-5527.
99. Tseng, C.-H., Tseng, I.-H., Huang, Y.-P., Hsu, Y.-T., Leu, J., Tu, K.-N., Chen, C., 2020, *Kinetic study of grain growth in highly (111)-preferred nanotwinned copper films*, Materials Characterization, 168, 110545.
100. Zhao, X., Lu, C., Tieu, A.K., Pei, L., Zhang, L., Cheng, K., Huang, M., 2016, *Strengthening mechanisms and dislocation processes in <111> textured nanotwinned copper*, Materials Science and Engineering: A, 676, pp. 474-486.
101. Liu, C.-M., Lin, H.-W., Huang, Y.-S., Chu, Y.-C., Chen, C., Lyu, D.-R., Chen, K.-N., Tu, K.-N., 2015, *Low-temperature direct copper-to-copper bonding enabled by creep on (111) surfaces of nanotwinned Cu*, Scientific Reports, 5, 9734.
102. Shie, K.C., Juang, J.-Y., Chen, C., 2019, *Instant Cu-to-Cu direct bonding enabled by <111>-oriented nanotwinned Cu bumps*, Japanese Journal of Applied Physics, 59(5), pp. 53-58.
103. Lu, T., Wang, P., Cheng, Y., Yen, Y., Wu, S., 2024, *Enhanced nanotwinned copper bonding through epoxy-induced copper surface modification*, Nanomaterials, 14(9), 771.